Engineering Applications of Artificial Intelligence 116 (2022) 105407

Contents lists available at ScienceDirect

Engineering Applications of Artificial Intelligence

journal homepage: www.elsevier.com/locate/engappai

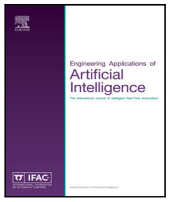

A distance of quantum mass function and its application in multi-source information fusion method based on discount coefficient

Lipeng Pan [a], Xiaozhuan Gao [a,d], Yong Deng [a,b,c,d,*]

[a] Institute of Fundamental and Frontier Science, University of Electronic Science and Technology of China, Chengdu, 610054, China
[b] School of Education, Shaanxi Normal University, Xi'an, 710062, China
[c] School of Knowledge Science, Japan Advanced Institute of Science and Technology, Nomi, Ishikawa 923-1211, Japan
[d] Department of Management, Technology, and Economics, ETH Zurich, Zurich, Switzerland

ARTICLE INFO

Keywords:
Evidence theory
Quantum mass function
Distance measure
Multi-source information fusion

ABSTRACT

Distance measures provide a novel perspective for measuring the difference or consistency between bodies of evidence, which have been used in a wide range of fields. However, under the framework of quantum mass function, existing distances cannot measure the difference. Hence, this paper formulates a new distance measure, referred to as the distance of the quantum mass functions. The purpose of this distance measure is to quantify the difference between quantum mass functions. It can be demonstrated mathematically that it is a strict distance measure that satisfies the nonnegativity, symmetry, definiteness, triangle inequality. The proposed distance measure is a generalization of the classical evidence distance, and it introduces the concept of Minkowski distance as well. It is therefore not only able to reflects the difference of discord and non-specificity in the mass functions, but it also has the advantage of Minkowski distance, as well as high compatibility. Moreover, A number of numerical examples are also provided to illustrate its properties and advantages. Using the proposed distance measure, we design a new information fusion method based on the discount coefficient within a complex framework. As a further investigation, the proposed fusion method is applied to several data sets experiments and results indicate that compared to other methods, it has a certain potential in the field of multi-source information fusion under the framework of evidence theory.

1. Introduction

As a matter of fact, uncertainty plays an essential role in philosophy, economics, information theory, finance and sociology. So, an effective and reasonable representation of uncertainty can facilitate our understanding of the real world (Yager, 2022; Wang et al., 2021b; Bouhamed et al., 2020; Cao et al., 2021a). To date, there are many methods for dealing with uncertainty, such as probability theory (Laplace, 1812), fuzzy sets (Zadeh, 1965), Dempster–Shafer evidence theory (Dempster, 1967; Shafer, 1976), evidence reasoning (Fu et al., 2021; Chang et al., 2020), random permutation set (Deng, 2022), entropy (Buono and Longobardi, 2020; Che et al., 2022) probabilistic linguistic term sets (Wang et al., 2021c) and extension theories (Yi et al., 2019; Cuzzolin, 2020; Solaiman et al., 2021). As a branch of probability theory, Dempster–Shafer evidence theory (D–S evidence theory) has been gaining interest in these studies since it describes the unknown and imprecise information by assigning the information into a power set (Jousselme et al., 2021; Xiaojing et al., 2022). Moreover, Dempster rule of combination combines information from multiple evidence sources for the same target, which exhibits fault tolerance (Liao et al., 2020). Consequently, it has been used in a wide variety of fields, such as multi-criteria decision-making (Surathong et al., 2018; Khalaj et al., 2020; Xiao et al., 2022), risk assessment (Chen and Deng, 2022; Wang et al., 2022a,b), Multi-source information fusion (Ghosh et al., 2021; Deng and Wang, 2021; Dong et al., 2021), reliability analysis (Gao et al., 2021b; Wang et al., 2021a; Gao et al., 2021c), target recognition (Porebski et al., 2018; Chen and Cai, 2022; Zhu and Xiao, 2021), pattern classification (Song et al., 2022; Xiao and Pedrycz, 2022; Liu et al., 2020), time series (Song and Xiao, 2022; Cui et al., 2022; Mi and Kang, 2020) and hybrid field (Ju et al., 2021; Dong et al., 2020; Cao et al., 2021b).

Traditionally, evidence theory has been able to manage the uncertainty in the classic application environment. However, when faced with periodic data or multi-dimensional information, the ability of traditional evidence theory to process that information is insufficient. This leads to the development of a generalized evidence theory described in Gao and Deng (2019). Generalized evidence theory defines the mass function in terms of quantum probability and renames it quantum mass function. Essentially, it describes the uncertainty within a complex framework by amplitude and phase angle. Additionally, some studies extended to the complex plane previously, including, but

* Corresponding author at: Institute of Fundamental and Frontier Science, University of Electronic Science and Technology of China, Chengdu, 610054, China.
E-mail address: dengentropy@uestc.edu.cn (Y. Deng).

https://doi.org/10.1016/j.engappai.2022.105407
Received 7 March 2022; Received in revised form 5 August 2022; Accepted 28 August 2022
Available online 16 September 2022
0952-1976/

not limited to, the fuzzy set theory (Ramot et al., 2002; Alkouri and Salleh, 2012; Ullah et al., 2020). In the real plane, these methods effectively describe the uncertain information (Janani et al., 2022; Mahmood and Ur Rehman, 2022). Despite this, there are also some problems that limit the further application of these studies. Consider the quantum mass function and classic mass function as an example. Many studies have been performed for distance measure between the classic mass functions, while little has been done on measuring distance between the quantum mass functions. In the real valued framework, Jousselme and Bossé first define the distance between two bodies of evidence, named the evidence distance (Jousselme et al., 2001). Evidence distance is based on Jacc matrix and Euclidean distance to effectively measure differences between bodies of evidence, which is a strict distance measure (Jousselme and Maupin, 2012). From the perspective of entropy, Xiao extends Jensen–Shannon divergence from probability space to evidence or power space and then define belief Jensen–Shannon divergence, which measures the difference of support degree between the same proposition (Xiao, 2019). Gao et al. present the concept of divergence of information volume based on the idea of splitting information volume (Gao et al., 2022). The value of divergence can reflect both differences in support degree for the same proposition as well as differences of elements between the proposition. As well as having their own advantages, these works are effective in measuring the difference between mass functions. However, none of these studies has been able to measure the difference between quantum mass functions on the complex plane. Thus, the primary motivation for this work is the development of a reasonable distance measure for reflecting the difference between quantum mass functions in a complex valued environment.

Hence, as a complement to the classic evidence distance (Jousselme distance) (Jousselme et al., 2001), this paper examines a distance of quantum mass functions (QMD). It is proposed that a distance measure be developed that takes into account the difference between quantum mass functions. Specifically, it not only considers the discord and non-specificity of mass function, but also has the advantage of Minkowski distance. Furthermore, this paper also uses some mathematical derivation to demonstrate the properties of proposed distance measure (nonnegativity, symmetry, definiteness, triangle inequality), i.e, it is the strict distance metric. When the quantum mass function degenerates to the classical mass functions, the proposed distance measure will degenerate into a class distance of mass functions. A further clarification is that if $p = 2$, the proposed distance measure will degenerate the classic evidence distance. Therefore, QMD not only effectively measures the difference between quantum mass functions, but also has high compatibility. Further, this paper designs a new multi-source information fusion method based on the discount coefficient in the complex framework. We then apply this fusion method to recognize unknown targets in the data sets. The results of experiments on some data sets indicate that compared to other methods, the new method has better recognition performance for unknown targets.

Here are some of the main contributions of this work:

- QMD is first proposed to quantify the difference between quantum mass functions. it takes into account not only considers the difference of support degree between the same proposition in the quantum mass functions, but also interrelation of the elements in proposition. Additionally, it is the strict distance metric, which satisfies the nonnegativity, symmetry, definiteness and triangle inequality.
- The proposed distance measure that combines the advantages of Minkowski distance and classical evidence distance. It can be applied to complex space as well as real space. Moreover, it provides a potential option for distance measure of uncertain information in other theories.
- A multi-source information fusion method based on the discount coefficient within the complex framework is designed for the first time, and experimental results of data sets show that the proposed method has a higher recognition rate within the framework of evidence theory.

2. A distance of Quantum mass functions in the complex framework

Prior to getting into the main topic of this article, some preliminaries regarding quantum mass function and evidence distance are introduced.

Definition 2.1 (*Quantum Mass Function, Gao and Deng, 2019*)**.** In the frame of discernment $\Theta = \{A_1, A_2, \ldots, A_n\}$, a quantum mass function (QM) $\mathbb{M}$ is described as follows:

$$\mathbb{M}(A_j) = a_{A_j} \cdot e^{i \cdot \theta_{A_j}} \tag{1}$$

which should satisfy:

$$\mathbb{M}(\emptyset) = 0 \tag{2}$$

$$0 \le |\mathbb{M}(A_j)| \le 1 \tag{3}$$

$$\sum_{A_j \subseteq 2^\Theta} |\mathbb{M}(A_j)| = 1 \tag{4}$$

where $\mathbb{M}(A_j)$ is the amplitude of the Euler formula, and the $|\mathbb{M}(A_j)| = a^2$ represents the quantum probability. θ_{A_j} represents the angle phase of an event A_j, which varies form the 0° to 360°. Moreover, Eq. (1) is also represented by using the complex number $\mathbb{M}(A_j) = x_{A_j} + y_{A_j} \cdot i$, $x = a_{A_j} \cdot cos(\theta_{A_j})$, $y = a_{A_j} \cdot sin(\theta_{A_j})$. When angle phase is 0, the quantum mass function degenerates the classical mass function. Some studies have been conducted concerning quantum mass functions, which have been applied to expert evaluation system (Gao and Deng, 2021; Gao et al., 2021a).

Definition 2.2 (*Dempster Rule of Combination of Quantum Mass Functions, (DRC-QM), Gao and Deng, 2019*)**.** For two quantum mass functions $\mathbb{M}_1$ and $\mathbb{M}_2$, the orthogonal sum is described as follows:

$$\mathbb{M}'\left(F_k\right) = \begin{cases} \sum_{F_m \cap F_n = F_k} \mathbb{M}_1\left(F_m\right) \times \mathbb{M}_2\left(F_n\right) & F_k \neq \emptyset \\ 0 & F_k = \emptyset \end{cases} \tag{5}$$

then $\mathbb{M}\left(F_k\right) = \sqrt{\frac{\left(\mathbb{M}'(F_k)\right)^2}{\sum_{F_k \subseteq 2^\Theta} |\mathbb{M}'(F_k)|}}$, and conflict coefficient $K = 1 - \sum_{F_k \subseteq 2^\Theta} \left|\mathbb{M}'\left(F_k\right)\right|$, which is another expression of the combination rule for the quantum mass functions.

Definition 2.3 (*Jousselme Distance, Jousselme et al., 2001*)**.**

$$d\left(m_1, m_2\right) = \sqrt{\frac{\left|\left(m_1 - m_2\right)^T \mathbb{W}\left(m_1 - m_2\right)\right|}{2}} \tag{6}$$

where m_1 and m_2 are two mass functions in the real-valued framework, $\mathbb{W}$ is conducted by the Jaccard index $\mathbb{J} = \frac{|F_m \cap F_n|}{|F_m \cup F_n|}$.

A distance of quantum mass functions is then proposed, which is referred to as QMD in short. The proposed distance measure corresponds to the extension of classical evidence distance combined with Minkowski distance. It can be applied to either real space or complex space. As a result, it is highly compatible. It also satisfies the axiom of distance.

2.1. Distance measure of quantum mass functions

Suppose there are two QMs ($\mathbb{M}_1$ and $\mathbb{M}_2$), the distance between $\mathbb{M}_1$ and $\mathbb{M}_2$ is detailed as follows.

$$\begin{aligned} \mathbb{D}^p\left(\mathbb{M}_1, \mathbb{M}_2\right) &= \frac{\left[\left((\mathbb{U}\mathbb{M}_1 - \mathbb{U}\mathbb{M}_2)^{\frac{p}{2}}\right)'\left((\mathbb{U}\mathbb{M}_1 - \mathbb{U}\mathbb{M}_2)^{\frac{p}{2}}\right)\right]^{\frac{1}{p}}}{\left[\left(\mathbb{M}_1^{\frac{p}{2}}\right)'\left(\mathbb{M}_1^{\frac{p}{2}}\right) + \left(\mathbb{M}_2^{\frac{p}{2}}\right)'\left(\mathbb{M}_2^{\frac{p}{2}}\right)\right]^{\frac{1}{p}}} \\ &= \frac{\left[\left((\mathbb{U}(\mathbb{M}_1 - \mathbb{M}_2))^{\frac{p}{2}}\right)'\left((\mathbb{U}(\mathbb{M}_1 - \mathbb{M}_2))^{\frac{p}{2}}\right)\right]^{\frac{1}{p}}}{\left[\left(\mathbb{M}_1^{\frac{p}{2}}\right)'\left(\mathbb{M}_1^{\frac{p}{2}}\right) + \left(\mathbb{M}_2^{\frac{p}{2}}\right)'\left(\mathbb{M}_2^{\frac{p}{2}}\right)\right]^{\frac{1}{p}}} \end{aligned} \tag{7}$$

where $\mathbb{U}$ represents the Cholesky decomposition of the matrix $\mathbb{W}$, $\mathbb{W} = \mathbb{U}'\mathbb{U}$. $\mathbb{W}$ is the Jaccard matrix between two quantum mass functions. The p is the integer which is more greater than 1. For ease of expression, $\mathbb{D}^p\left(\mathbb{M}_1, \mathbb{M}_2\right)$ is also simplified to $\mathbb{D}^p_{12}$. The $\mathbb{M}_1 - \mathbb{M}_2$ is a vector that is formed by difference between the same components of $\mathbb{M}_1$ and $\mathbb{M}_2$. Moreover, the proposed distance measure is highly compatible, and explained in detail as follows:

- When the $p = 2$, $\mathbb{W}$ is conducted by the Jacc index, $\mathbb{W}_{mn} = \mathbb{J} = \frac{|F_m \cap F_n|}{|F_m \cup F_n|}$, the proposed distance measure degenerates to the extension of classical evidence distance under complex framework.

$$\begin{aligned}\mathbb{D}^p\left(\mathbb{M}_1, \mathbb{M}_2\right) &= \frac{\left[(\mathbb{U}\mathbb{M}_1 - \mathbb{U}\mathbb{M}_2)'(\mathbb{U}\mathbb{M}_1 - \mathbb{U}\mathbb{M}_2)\right]^{\frac{1}{2}}}{(\mathbb{M}_1'\mathbb{M}_1 + \mathbb{M}_2'\mathbb{M}_2)^{\frac{1}{2}}} \\ &= \frac{\left[(\mathbb{U}(\mathbb{M}_1 - \mathbb{U}\mathbb{M}_2))'(\mathbb{U}(\mathbb{M}_1 - \mathbb{U}\mathbb{M}_2))\right]^{\frac{1}{2}}}{(\mathbb{M}_1'\mathbb{M}_1 + \mathbb{M}_2'\mathbb{M}_2)^{\frac{1}{2}}} \\ &= \frac{\left[(\mathbb{M}_1 - \mathbb{U}\mathbb{M}_2)'\mathbb{U}'\mathbb{U}(\mathbb{M}_1 - \mathbb{M}_2)\right]^{\frac{1}{2}}}{(\mathbb{M}_1'\mathbb{M}_1 + \mathbb{M}_2'\mathbb{M}_2)^{\frac{1}{2}}} \\ &= \left[\frac{(\mathbb{M}_1 - \mathbb{M}_2)'\mathbb{W}(\mathbb{M}_1 - \mathbb{M}_2)}{\mathbb{M}_1'\mathbb{M}_1 + \mathbb{M}_2'\mathbb{M}_2}\right]^{\frac{1}{2}}\end{aligned} \tag{8}$$

- As the quantum mass functions degenerate to a mass functions of real space, the proposed distance measure has the following form.
  - When the $p = 2$ and $\mathbb{W}$ is the Jaccard matrix, the proposed distance measure will degenerate to the classical evidence distance.
  - When the $p = 1$, and $\mathbb{W}$ is unit matrix, the proposed distance measure will degenerate to the Manhattan distance.
  - When the $p = 2$, and $\mathbb{W}$ is unit matrix, the proposed distance measure will degenerate to the Euclidean distance.
  - When the $p \to +\infty$, and $\mathbb{W}$ is unit matrix, the proposed distance measure will degenerate to the Chebyshev distance.

Obviously, it can be seen from Eq. (7) that distance reflects the difference between quantum mass functions. The greater the difference between quantum mass functions, the greater the distance. A smaller difference between quantum mass functions corresponds to a smaller distance. Furthermore, it also has the following properties:

Property 1. *Nonnegativity:* $\mathbb{D}^p(\mathbb{M}_1, \mathbb{M}_2) \geq 0$.

Property 2. *Symmetry:* $\mathbb{D}^p(\mathbb{M}_1, \mathbb{M}_2) = \mathbb{D}^p(\mathbb{M}_2, \mathbb{M}_1)$.

Property 3. *Definiteness:* $\mathbb{D}^p(\mathbb{M}_1, \mathbb{M}_2) = 0 \Leftrightarrow \mathbb{M}_1 = \mathbb{M}_2$.

Property 4. *Triangle inequality:* $\mathbb{D}^p(\mathbb{M}_1, \mathbb{M}_2) \leq \mathbb{D}^p(\mathbb{M}_1, \mathbb{M}_3) + \mathbb{D}^p(\mathbb{M}_2, \mathbb{M}_3)$.

Next, here are the specific proofs of properties.

Proof 1. Suppose the $a = ((\mathbb{U}(\mathbb{M}_1 - \mathbb{M}_2))^{\frac{p}{2}})$, which is represented as $a = [a_1 + b_1 \cdot i, a_2 + b_2 \cdot i, \ldots, a_n + b_n \cdot i]^T$. Then the $a' = [a_1 - b_1 \cdot i, a_2 - b_2 \cdot i, \ldots, a_n - b_n \cdot i]$. Hence $a' \cdot a \geq 0$. Similarly, the $(\mathbb{M}_1^{\frac{p}{2}})'(\mathbb{M}_1^{\frac{p}{2}})$ is also greater than or equal to 0. Hence, QMD satisfies the property of non-negativity. □

Proof 2. The denominator of $\mathbb{D}^p(\mathbb{M}_1, \mathbb{M}_2)$ and $\mathbb{D}^p(\mathbb{M}_2, \mathbb{M}_1)$ is equal. The relationship of $\mathbb{D}^p(\mathbb{M}_1, \mathbb{M}_2)$ and $\mathbb{D}^p(\mathbb{M}_2, \mathbb{M}_1)$ are obtained by analyzing the molecules. Assume the $d_{12} = (\mathbb{U}\mathbb{M}_1 - \mathbb{U}\mathbb{M}_2)^{\frac{p}{2}}$, $d_{21} = (\mathbb{U}\mathbb{M}_2 - \mathbb{U}\mathbb{M}_1)^{\frac{p}{2}}$. For

$$d_{12} = \begin{bmatrix} a_1 + b_1 \cdot i \\ a_2 + b_2 \cdot i \\ \vdots \\ a_n + b_n \cdot i \end{bmatrix}, d_{12}^{p/2} = \begin{bmatrix} a_{11} + b_{11} \cdot i \\ a_{22} + b_{22} \cdot i \\ \vdots \\ a_{nn} + b_{nn} \cdot i \end{bmatrix}$$

$$(d_{12}^{p/2})' * d_{12}^{p/2} = a_{11}^2 + b_{11}^2 + a_{22}^2 + b_{22}^2 + \cdots + a_{nn}^2 + b_{nn}^2$$

$$d_{21} = \begin{bmatrix} -(a_1 + b_1 \cdot i) \\ -(a_2 + b_2 \cdot i) \\ \vdots \\ -(a_n + b_n \cdot i) \end{bmatrix}, d_{21}^{p/2} = \begin{bmatrix} ((-1)^{p/2})(a_{11} + b_{11} \cdot i) \\ ((-1)^{p/2})(a_{22} + b_{22} \cdot i) \\ \vdots \\ ((-1)^{p/2})(a_{nn} + b_{nn} \cdot i) \end{bmatrix}$$

$$d_{21}^{p/2} = \begin{cases} \begin{bmatrix} \mp b_{11} \pm a_{11} \cdot i \\ \mp b_{22} \pm a_{22} \cdot i \\ \vdots \\ \mp b_{nn} \pm a_{nn} \cdot i \end{bmatrix}, \text{ if } p \text{ is odd} \\ \begin{bmatrix} \pm a_{11} \pm b_{11} \cdot i \\ \pm a_{22} \pm b_{22} \cdot i \\ \vdots \\ \pm a_{nn} \pm b_{nn} \cdot i \end{bmatrix}, \text{ if } p \text{ is even} \end{cases}$$

$$(d_{21}^{p/2})' d_{21}^{p/2} = b_{11}^2 + a_{11}^2 + b_{22}^2 + a_{22}^2 + \cdots + b_{nn}^2 + a_{nn}^2$$

Hence, the property of symmetry is proved. □

Proof 3. When $\mathbb{M}_1 = \mathbb{M}_2$, the distance $\mathbb{D}^p(\mathbb{M}_1, \mathbb{M}_2) = 0$. Besides, $\left[(\mathbb{M}_1^{\frac{p}{2}})'(\mathbb{M}_1^{\frac{p}{2}}) + (\mathbb{M}_2^{\frac{p}{2}})'(\mathbb{M}_2^{\frac{p}{2}})\right]^{\frac{1}{p}}$ is also greater than 0.

Hence, if $\mathbb{D}^p(\mathbb{M}_1, \mathbb{M}_2) = 0$, the $\left[((\mathbb{U}\mathbb{M}_1 - \mathbb{U}\mathbb{M}_2)^{\frac{p}{2}})'((\mathbb{U}\mathbb{M}_1 - \mathbb{U}\mathbb{M}_2)^{\frac{p}{2}})\right]^{\frac{1}{p}}$ is equal to 0, which indicates $\mathbb{M}_1 = \mathbb{M}_2$. □

Proof 4. Suppose

$$d_{12} = ((\mathbb{U}\mathbb{M}_1 - \mathbb{U}\mathbb{M}_2)^{\frac{p}{2}})'(\mathbb{U}\mathbb{M}_1 - \mathbb{U}\mathbb{M}_2)^{\frac{p}{2}} = \sum(a_i^2 + b_i^2)$$

$$d_{13} = ((\mathbb{U}\mathbb{M}_1 - \mathbb{U}\mathbb{M}_3)^{\frac{p}{2}})'(\mathbb{U}\mathbb{M}_1 - \mathbb{U}\mathbb{M}_3)^{\frac{p}{2}} = \sum(c_i^2 + d_i^2)$$

$$d_{23} = ((\mathbb{U}\mathbb{M}_2 - \mathbb{U}\mathbb{M}_3)^{\frac{p}{2}})'(\mathbb{U}\mathbb{M}_2 - \mathbb{U}\mathbb{M}_3)^{\frac{p}{2}} = \sum(e_i^2 + f_i^2)$$

Fig. 1 gives the specific explanation about $d_{13}+d_{23} \geq d_{12}$. From $d_{12} = \sum(a_i^2 + b_i^2)$, it can be seen that d_{12} is the sum of 2^n complex numbers. Hence, in the Fig. 1, taking the certain complex number of $\mathbb{M}_1$, $\mathbb{M}_2$, $\mathbb{M}_3$ as an example to better analyze the inequality $d_{13}+d_{23} \geq d_{12}$. According to the properties of the triangle, $d_{13} + d_{23} \geq d_{12}$ is obtained.

$$m_1 = (\mathbb{M}_1^{\frac{p}{2}})'(\mathbb{M}_1^{\frac{p}{2}}) \quad m_2 = (\mathbb{M}_2^{\frac{p}{2}})'(\mathbb{M}_2^{\frac{p}{2}})$$

$$m_3 = (\mathbb{M}_3^{\frac{p}{2}})'(\mathbb{M}_3^{\frac{p}{2}}) \quad \mathbb{D}_{12}^p = \left[\frac{d_{12}}{m_1 + m_2}\right]^{1/p}$$

$$\mathbb{D}_{13}^p = \left[\frac{d_{13}}{m_1 + m_3}\right]^{1/p} \quad \mathbb{D}_{23}^p = \left[\frac{d_{23}}{m_2 + m_3}\right]^{1/p}$$

$$D_{12} = \frac{d_{12}}{m_1 + m_2} \quad D_{13} = \frac{d_{13}}{m_1 + m_3} \quad D_{23} = \frac{d_{23}}{m_2 + m_3}$$

$$\begin{aligned} D_{13} + D_{23} - D_{12} &= \frac{d_{13}}{m_1 + m_3} + \frac{d_{23}}{m_2 + m_3} - \frac{d_{12}}{m_1 + m_2} \\ &= \frac{(m_1 + m_2)(m_2 + m_3)d_{13} + (m_1 + m_2)(m_1 + m_3)d_{23}}{(m_1 + m_2)(m_1 + m_3)(m_2 + m_3)} \\ &\quad - \frac{(m_1 + m_3)(m_2 + m_3)d_{12}}{(m_1 + m_2)(m_1 + m_3)(m_2 + m_3)} \end{aligned}$$

$$\begin{aligned} D &= (m_1 + m_2)(m_2 + m_3)d_{13} + (m_1 + m_2)(m_1 + m_3)d_{23} \\ &\quad - (m_1 + m_3)(m_2 + m_3)d_{12} \\ &= (m_1 m_2 + m_1 m_3 + m_2 m_3)(d_{13} + d_{23} - d_{12}) + (m_2)^2 d_{13} \\ &\quad + (m_1)^2 d_{23} - (m_3)^2 d_{12} \end{aligned}$$

$$D_{13} + D_{23} - D_{12} \geq 0 \Rightarrow \mathbb{D}_{13}^p + \mathbb{D}_{23}^p \geq \mathbb{D}_{12}^p$$

Thus, the triangle inequality is proved. □

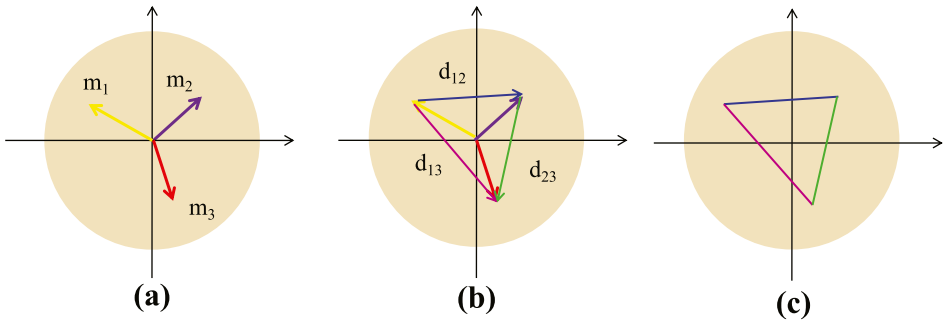

Fig. 1. The explanation of $d_{13} + d_{23} \geq d_{12}$.

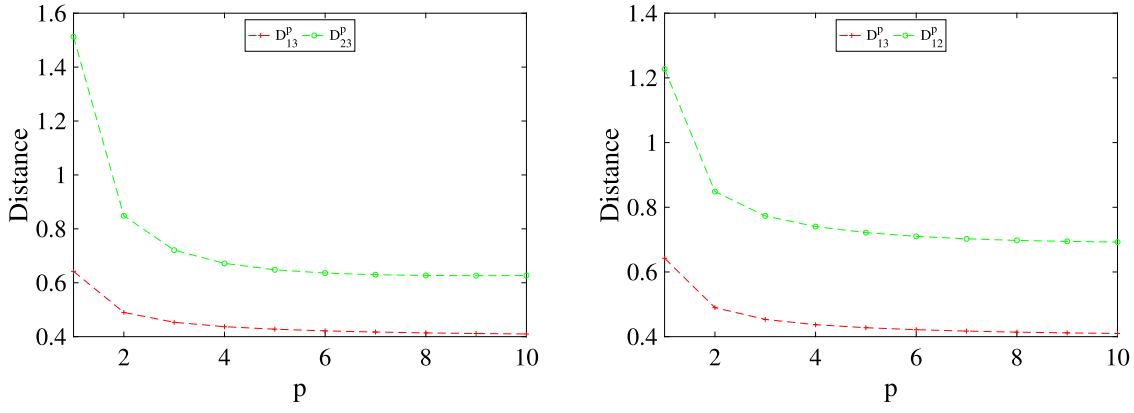

(a) $\mathbb{D}_{13}^{p}$ and $\mathbb{D}_{23}^{p}$ (b) $\mathbb{D}_{13}^{p}$ and $\mathbb{D}_{12}^{p}$

Fig. 2. The distances in Example 2.1 with different p.

2.2. Numerical example

For the purpose of explaining the properties and characteristics of the proposed distance measure, some numerical examples are provided in this subsection.

Example 2.1. The frame of discernment is $\Theta = \{A, B, C, D, E\}$, the $\mathbb{M}_1$, $\mathbb{M}_2$, $\mathbb{M}_3$ are as follows.

$$\mathbb{M}_1(A, B) = \sqrt{0.72}e^{j45^\circ}, \mathbb{M}_1(\Theta) = \sqrt{0.28}e^{j90^\circ}$$

$$\mathbb{M}_2(D, E) = \sqrt{0.72}e^{j45^\circ}, \mathbb{M}_2(\Theta) = \sqrt{0.28}e^{j90^\circ}$$

$$\mathbb{M}_3(A, B, C) = \sqrt{0.72}e^{j45^\circ}, \mathbb{M}_1(\Theta) = \sqrt{0.28}e^{j90^\circ}$$

By analyzing the Example 2.1, it can be seen that $\mathbb{M}_1$ and $\mathbb{M}_3$ both have the more greater support degree for event A than $\mathbb{M}_2$, this leads to the $\mathbb{M}_1$ is more similar to the $\mathbb{M}_3$ than the $\mathbb{M}_2$. The results distance measure should satisfy $\mathbb{D}_{13}^{p} < \mathbb{D}_{23}^{p}$, $\mathbb{D}_{13}^{p} < \mathbb{D}_{12}^{p}$. Additionally, these results cannot vary with the changes of p, and Fig. 2 illustrates this in more detail.

In Fig. 2 , the value of p changes from 1 to 10. Fig. 2(a) shows the distance between $\mathbb{M}_1$ and $\mathbb{M}_3$, between $\mathbb{M}_2$ and $\mathbb{M}_3$. Fig. 2(b) shows the distance between $\mathbb{M}_1$ and $\mathbb{M}_3$, between $\mathbb{M}_1$ and $\mathbb{M}_2$. It can be seen that no matter how p changes, the result is intuitive. Hence, it can be seen that the proposed method is reasonable.

Also, this example is also used to verify the triangle inequality, shown in Fig. 3. D_{jk}^{q} represents the distance between $\mathbb{M}_j$ and $\mathbb{M}_k$. Besides, the value of p changes from 1 to 10. By analyzing the Fig. 3, it is found that the triangle inequality is satisfied no matter how q changes.

Example 2.2. Suppose there is a frame of discernment is $\Theta = \{A, B\}$, the $\mathbb{M}_1$, $\mathbb{M}_2$ are two quantum mass functions:

$$\mathbb{M}_1(A) = \frac{x}{\sqrt{x^2 + 2 \times y^2 + (1-x)^2}} - \frac{y}{\sqrt{x^2 + 2 \times y^2 + (1-x)^2}}i$$

$$\mathbb{M}_1(x_1) = \frac{1-x}{\sqrt{x^2 + 2 \times y^2 + (1-x)^2}} + \frac{y}{\sqrt{x^2 + 2 \times y^2 + (1-x)^2}}i$$

$$\mathbb{M}_2(A) = \frac{1-x}{\sqrt{x^2 + 2 \times y^2 + (1-x)^2}} - \frac{y}{\sqrt{x^2 + 2 \times y^2 + (1-x)^2}}i$$

$$\mathbb{M}_2(x_2) = \frac{x}{\sqrt{x^2 + 2 \times y^2 + (1-x)^2}} + \frac{y}{\sqrt{x^2 + 2 \times y^2 + (1-x)^2}}i$$

Example 2.2 is obtained in Xiao (2020), it is normalized based on Example 6 from Xiao (2020). In this example, $x_1, x_2 \subseteq \{A, B, AB\}$, and the x and y varies in the range of $[0, 1]$.

Firstly, when the $\mathbb{M}_j$ degenerates the classical mass function, that is to say, $y = 0$, the distance between $\mathbb{M}_1$ and $\mathbb{M}_2$ is shown in Fig. 4 with $p = 1$, $p = 2$, $p = 3$. Moreover, in Fig. 4 , $x_1 = A, B$ represents the $\mathbb{M}_1(A, B)$, $x_2 = A, B$ represents the $\mathbb{M}_2(A, B)$. Obviously, no matter how x changes, the distance is always greater than 0 or equal to 0, which is consistent with the property 1. Due the change of θ, here are three cases as follows.

Case 1: $\mathbb{M}_1(A)$, $\mathbb{M}_1(B)$ and $\mathbb{M}_2(A)$, $\mathbb{M}_2(B)$. In this case, it can be seen that the distance has the minimum value when $\mathbb{M}_1(A) = 0.7071$, $\mathbb{M}_1(B) = 0.7071$ and $\mathbb{M}_2(A) = 0.7071$, $\mathbb{M}_2(B) = 0.7071$, that is to say, $x = 0.5$. On the other hand, it can be known that there is the maximum value of distance when two quantum mass functions support completely different propositions. In other words, the distance is 1 when $x = 0$ ($\mathbb{M}_1(B) = 1$, $\mathbb{M}_2(A) = 1$) or $x = 1$ ($\mathbb{M}_1(A) = 1$, $\mathbb{M}_2(B) = 1$). Furthermore, it is obvious that the distance measure is symmetric with respect to $x = 0.5$.

Case 2: $\mathbb{M}_1(A)$, $\mathbb{M}_1(AB)$ and $\mathbb{M}_2(A)$, $\mathbb{M}_2(B)$. In this case, there is the maximum value of distance when $x = 1$ ($\mathbb{M}_1(A) = 1$, $\mathbb{M}_2(B) = 1$).

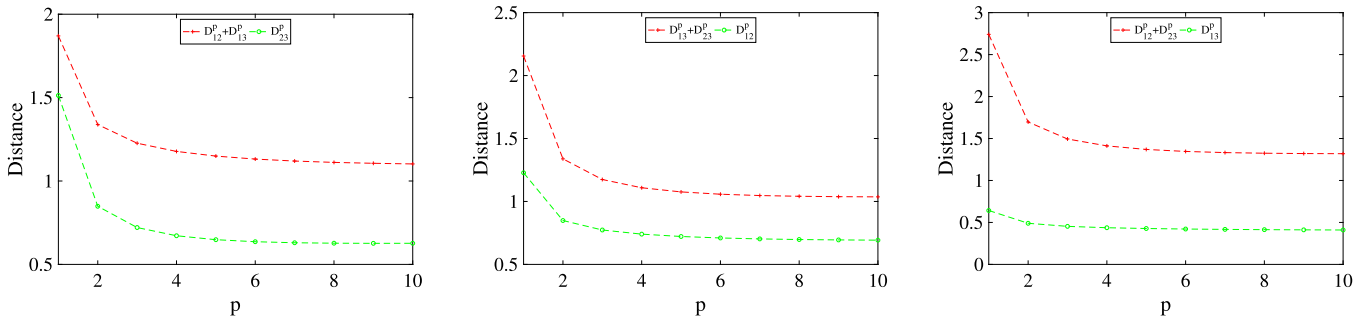

(a) $\mathbb{D}^p_{13}$ and $\mathbb{D}^p_{23}$ (b) $\mathbb{D}^p_{13}$ and $\mathbb{D}^p_{12}$ (c) $\mathbb{D}^p_{13}$ and $\mathbb{D}^p_{12}$

Fig. 3. The triangle inequality of distance in Example 2.1 with different p.

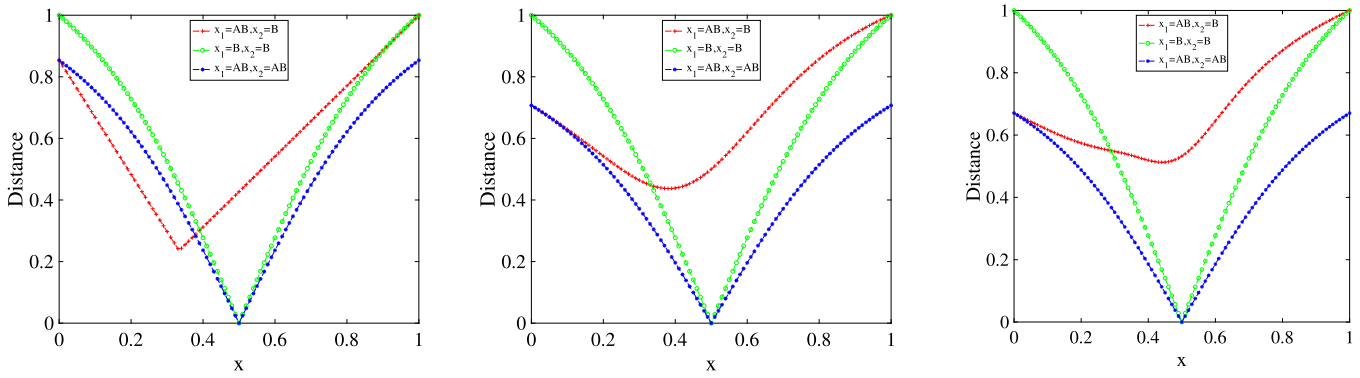

(a) $p = 1$ (b) $p = 2$ (c) $p = 3$

Fig. 4. The distance in Example 2.2 with $y = 0$.

Since the $\{B\}$ and $\{A, B\}$ have the intersection, the minimum value of distance measure is no longer 0.

Case 3: $\mathbb{M}_1(A)$, $\mathbb{M}_1(AB)$ and $\mathbb{M}_2(A)$, $\mathbb{M}_2(AB)$. In this case, it is clear that the value of distance with x from 0 to 1 is symmetry since the $\mathbb{M}_1$ and $\mathbb{M}_2$ have the same focal element. The distance measure in the Case 3 is more smaller or equal to the distance in the Case 1 because the $\{A, B\}$ and $\{A\}$ have the intersection. Also, there is the minimum value of distance when the $\mathbb{M}_1$ and $\mathbb{M}_2$ are same. Hence, it can be seen that the proposed distance measure is intuitive and reasonable. Next, discuss how x and y affect the distance measure between $\mathbb{M}_1$ and $\mathbb{M}_2$.

Case 1: Fig. 5 shows the distance measure between $\mathbb{M}_1(A)$, $\mathbb{M}_1(B)$ and $\mathbb{M}_2(A)$, $\mathbb{M}_2(B)$ with the $p = 1$, $p = 2$, $p = 3$. It can be seen that the distance measures are symmetrical with the variation of x and y. No matter how change of x and y, the distance is always more greater or equal than 0. When $x = 0.5$ and $y = 0$, in this case, the QM degenerates the classical mass functions, $\mathbb{M}_1$ and $\mathbb{M}_2$ are same, there is the minimum value of distance. When $x = 0.5$, the distance becomes the more and more greater with the increase of y. It can be seen that imaginary number plays an essential role in distance measure. When $x = 1$, $y = 0$, there is the maximum value of distance. Similarly, $x = 0$, $y = 1$, there is also the maximum value of distance.

Case 2: Fig. 6 shows the distance between $\mathbb{M}_1(A)$, $\mathbb{M}_1(AB)$ and $\mathbb{M}_2(A)$, $\mathbb{M}_2(B)$ with the $p = 1$, $p = 2$, $p = 3$. The change of distance with the x and y is different from the Case 1 since the $\mathbb{M}_1(AB)$ and $\mathbb{M}_2(B)$ have the same element B. Furthermore, $\mathbb{M}_1$ and $\mathbb{M}_2$ are not same no matter how change x and y, hence the distance is always greater than 0.

Case 3: Fig. 7 shows the distance between $\mathbb{M}_1(A)$, $\mathbb{M}_1(AB)$ and $\mathbb{M}_2(A)$, $\mathbb{M}_2(AB)$ with the change of x and y. In this case, the $\mathbb{M}_1$ and $\mathbb{M}_2$ have the same focal elements, the change trend of distance is similar with the Case 1. However, the distance of Case 3 is more smaller than the Case 1. The reason is that focal elements ($\{A\}$, $\{B\}$) of Case 1 are mutually exclusive, the focal elements ($\{A\}$, $\{AB\}$) of Case 3 have the interaction.

In general, there are the same change trends of distance for Case 1, Case 2 and Case 3 with different p. However, different p makes different value of distance. Therefore, choosing the right value of p will help us to analyze distance better.

Example 2.3. Suppose there are two quantum mass functions $\mathbb{M}_1$, $\mathbb{M}_2$.

$$\mathbb{M}_1(A) = \frac{0.1}{\sqrt{0.82 + 2 \cdot \alpha^2}} + \frac{\alpha}{\sqrt{0.82 + 2 \cdot \alpha^2}} i$$
$$\mathbb{M}_1(x_\omega) = \frac{0.9}{\sqrt{0.82 + 2 \cdot \alpha^2}} - \frac{\alpha}{\sqrt{0.82 + 2 \cdot \alpha^2}} i$$
$$\mathbb{M}_2(A) = \frac{0.9}{\sqrt{0.82 + 2 \cdot \alpha^2}} - \frac{\alpha}{\sqrt{0.82 + 2 \cdot \alpha^2}} i$$
$$\mathbb{M}_2(x_\omega) = \frac{0.1}{\sqrt{0.82 + 2 \cdot \alpha^2}} + \frac{\alpha}{\sqrt{0.82 + 2 \cdot \alpha^2}} i$$

The example can be found in Xiao (2020), which has been normalized. An overview of change in frame of discernment is shown in Table 1. The α settings for the $\mathbb{M}_1$ and $\mathbb{M}_2$ are 0, 0.1, 0.2, 0.3,respectively. It focuses mainly on the change of distance with the variation of frame of discernment in this example. The distance measure between $\mathbb{M}_1$ and $\mathbb{M}_2$ is shown in Fig. 8, where (a) represents the $p = 1$, (b) represents the $p = 2$, (c) represents the $p = 3$.

Case 1: When $\alpha = 0$, the $\mathbb{M}_1$ and $\mathbb{M}_2$ degenerates to the classical BPA, then the $\mathbb{M}_1(A) = 0.1104$, $\mathbb{M}_1(x_\omega) = 0.9939$, $\mathbb{M}_2(A) = 0.9939$, $\mathbb{M}_2(x_\omega) = 0.1104$. From the Fig. 8, it can be found that the distance is more and more greater with the increase of the size of subset x_ω. This result is intuitive and reasonable, since the larger difference is caused by the increased frame of discernment.

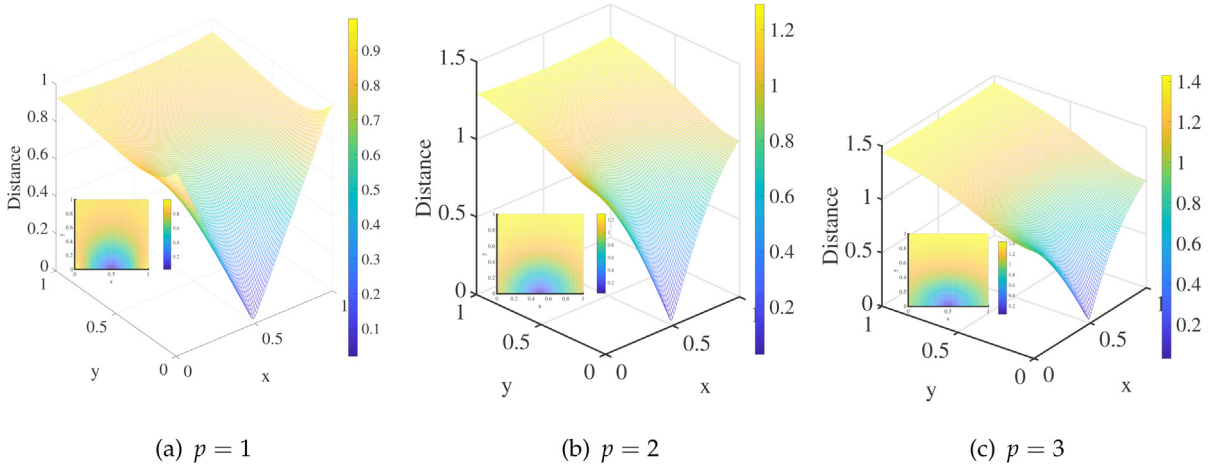

Fig. 5. The distance of Case 1 in Example 2.2 with the change of x and y.

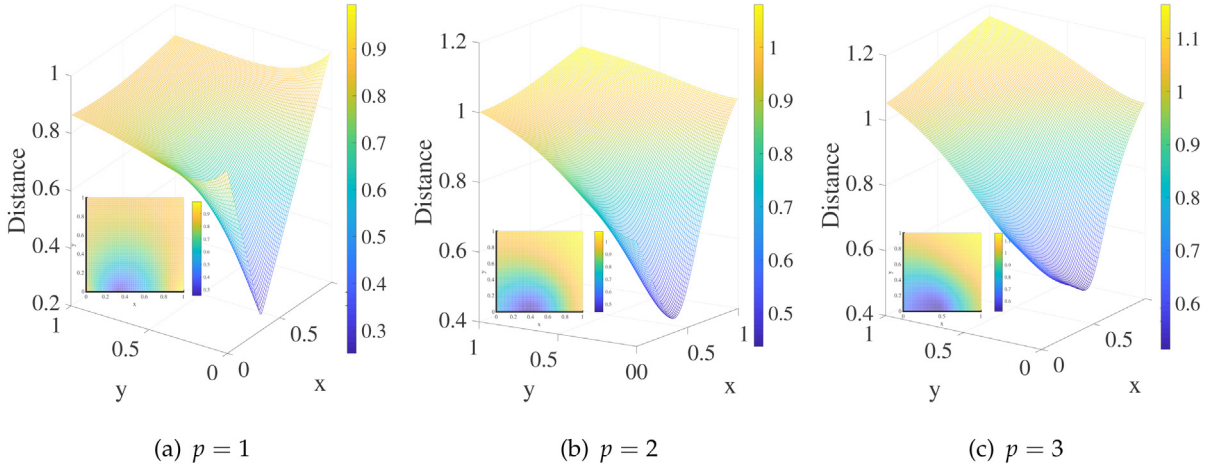

Fig. 6. The distance of Case 2 in Example 2.2 with the change of x and y.

Table 1
The variation of frame of discernment.

ω	x_ω
1	$\{A\}$
2	$\{A, B\}$
3	$\{A, B, C\}$
4	$\{A, B, C, D\}$
5	$\{A, B, C, D, E\}$
6	$\{A, B, C, D, E, F\}$
7	$\{A, B, C, D, E, F, G\}$
8	$\{A, B, C, D, E, F, G, H\}$
9	$\{A, B, C, D, E, F, G, H, I\}$
10	$\{A, B, C, D, E, F, G, H, I, J\}$

Case 2: When $\alpha = 0.1$, then the $\mathbb{M}_1(A) = 0.1091 + 0.1091i$, $\mathbb{M}_1(x_\omega) = 0.9820 - 0.1091i$, $\mathbb{M}_2(A) = 0.9820 - 0.1091i$, $\mathbb{M}_2(x_\omega) = 0.1091 + 0.1091i$.

Case 3: When $\alpha = 0.2$, then the $\mathbb{M}_1(A) = 0.1054 + 0.2108i$, $\mathbb{M}_1(x_\omega) = 0.9487 - 0.2108i$, $\mathbb{M}_2(A) = 0.9487 - 0.2108i$, $\mathbb{M}_2(x_\omega) = 0.1054 + 0.2108i$.

Case 4: When $\alpha = 0.3$, then the $\mathbb{M}_1(A) = 0.1000 + 0.3000i$, $\mathbb{M}_1(x_\omega) = 0.9000 - 0.3000i$, $\mathbb{M}_2(A) = 0.9000 - 0.3000i$, $\mathbb{M}_2(x_\omega) = 0.1000 + 0.3000i$.

By analyzing the *Case* 2 – –4, it also can be found that the distance becomes the more and more greater with the increase of the size of subset x_ω. It is indicates that the proposed distance measure is effective and reasonable. Besides, when $\alpha = 0$, the distance has the minimum value. Hence, the imaginary number plays an essential role in the distance measure. In addition, Fig. 9. (b) and (c) are more easy to analyze the difference between $\mathbb{M}_1$ and $\mathbb{M}_2$ with the change of α than Fig. 9(a).

3. A new multi-source information fusion method based on discount coefficient in complex framework

In this section, we present a new multi-source information fusion method based on the discount coefficient. This is the first time that the discount coefficient has been considered within a complex framework. Additionally, we apply the proposed fusion method to the data sets, and the experimental results demonstrate that the proposed method has certain advantages.

3.1. Method described

Since the discount coefficient is proposed by Shafer, it has attracted considerable attention in the field of dealing with evidence conflicts (Shafer, 1976). These works effectively solve the conflict problems of evidence theory in the real framework, and then promote the application of evidence theory in many fields, including but not limited to multi-source information fusion (Sarabi-Jamab and Araabi, 2018; Yan et al., 2021; Xiong et al., 2021). Therefore, the purpose of this subsection is to design a new multi-source information fusion method based on discount coefficients within the complex framework. Below is a description of specific process:

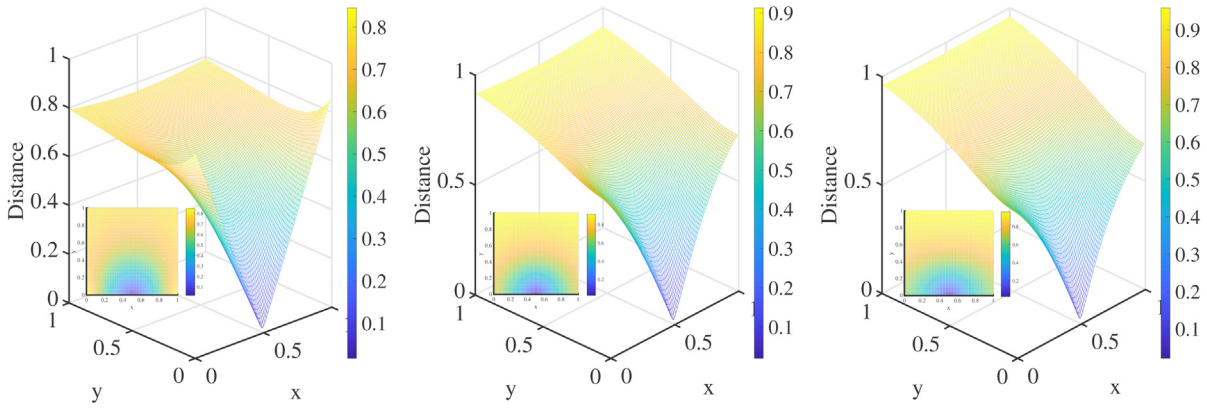

(a) $p = 1$ (b) $p = 2$ (c) $p = 3$

Fig. 7. The distance of Case 3 in Example 2.2 with the change of x and y.

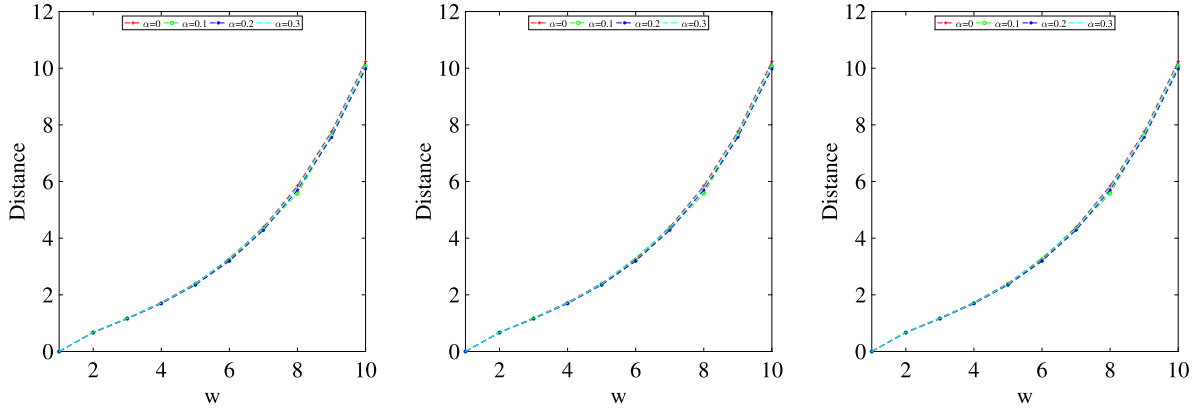

(a) $p = 1$ (b) $p = 2$ (c) $p = 3$

Fig. 8. The distance in Example 2.3.

Step 1: The distance measure $\mathbb{D}^p\left(\mathbb{M}_k, \mathbb{M}_1\right)$ between two bodies of evidence $\mathbb{M}_k$ and $\mathbb{M}_l$ is calculated by Eq. (7). Further, a matrix of distance measure $\overline{M} = \left[\mathbb{D}^p\left(\mathbb{M}_k, \mathbb{M}_l\right)\right]_{n\times n}$ is constructed as follows:

$$\overline{M} = \begin{bmatrix} 0 & \cdots & \mathbb{D}^p\left(\mathbb{M}_1, \mathbb{M}_l\right) & \cdots & \mathbb{D}^p\left(\mathbb{M}_1, \mathbb{M}_n\right) \\ \vdots & \cdots & \vdots & \cdots & \vdots \\ \mathbb{D}^p\left(\mathbb{M}_k, \mathbb{M}_1\right) & \cdots & 0 & \cdots & \mathbb{D}^p\left(\mathbb{M}_k, \mathbb{M}_n\right) \\ \vdots & \cdots & \vdots & \cdots & \vdots \\ \mathbb{D}^p\left(\mathbb{M}_n, \mathbb{M}_1\right) & \cdots & \mathbb{D}^p\left(\mathbb{M}_n, \mathbb{M}_l\right) & \cdots & 0 \end{bmatrix} \tag{9}$$

Step 2: Calculate the support degree of the body of evidence for $\mathbb{M}_k\,(k = 1, \ldots, n)$.

$$\overline{Sup_{\mathbb{M}_k}} = \sum_{l=1, l\neq k}^{n} 1 - \mathbb{D}^p\left(\mathbb{M}_k, \mathbb{M}_l\right) \tag{10}$$

Step 3: Determine the discount coefficient for each body of evidence $\mathbb{M}_k\,(k = 1, \ldots, n)$.

$$\overline{\alpha_k} = \sqrt{\frac{\overline{Sup_{\mathbb{M}_k}}}{\sum_{l=1}^{n} \overline{Sup_{\mathbb{M}_l}}}} \tag{11}$$

Step 4: Generate the discount mass function for each body of evidence $\mathbb{M}_k\,(k = 1, \ldots, n)$.

$$\overline{\alpha_k}\mathbb{M}_k = \begin{cases} \overline{\alpha_k} \times \mathbb{M}_k(A) & A \subseteq \Theta, A \neq \Theta \\ \sum\left(1 - \overline{\alpha_k}\right) \times \mathbb{M}_k(A) + \mathbb{M}_k(\Theta) & otherwise \end{cases} \tag{12}$$

Step 5: Normalize the discount mass function $\overline{\alpha_k}\mathbb{M}_k\,(k = 1, \ldots, n)$.

Table 2
Characteristics of the real data sets.

Dataset	Instances	Classes	Variables
Iris	150	3	4
Seeds	210	3	7
Algerian forest fires (AFF)	244	2	10
Breast Cancer	699	2	9
Credit Approval (CA)	690	2	15
Fertility Diagnosis (FD)	100	2	9

Step 6: Combine N discount mass functions in turn through Eq. (6).

$$\overline{CM} = \left(\left(\left(\left(\overline{\alpha_1}\mathbb{M}_1 \bigoplus \overline{\alpha_2}\mathbb{M}_2\right) \bigoplus \overline{\alpha_2}\mathbb{M}_2\right) \bigoplus \cdots\right) \bigoplus \overline{\alpha_n}\mathbb{M}_n\right) \tag{13}$$

Step 7: Though PPT rule to transformed $\overline{CM}$, and the proposition with the greatest support is selected as recognized target.

In order to better explain this method, its pseudo-code is shown in Algorithm 1.

3.2. Applications in data sets

In this subsection, we apply the multi-source information fusion method to the some data sets. After that, the proposed method is evaluated in terms of its performance in the data set environment.

Data set description: The data sets are from the UCI database (http://archive.ics.uci.edu/ml/index.php), including the Iris and Seeds data sets, and Table 2 provides details about these data sets.

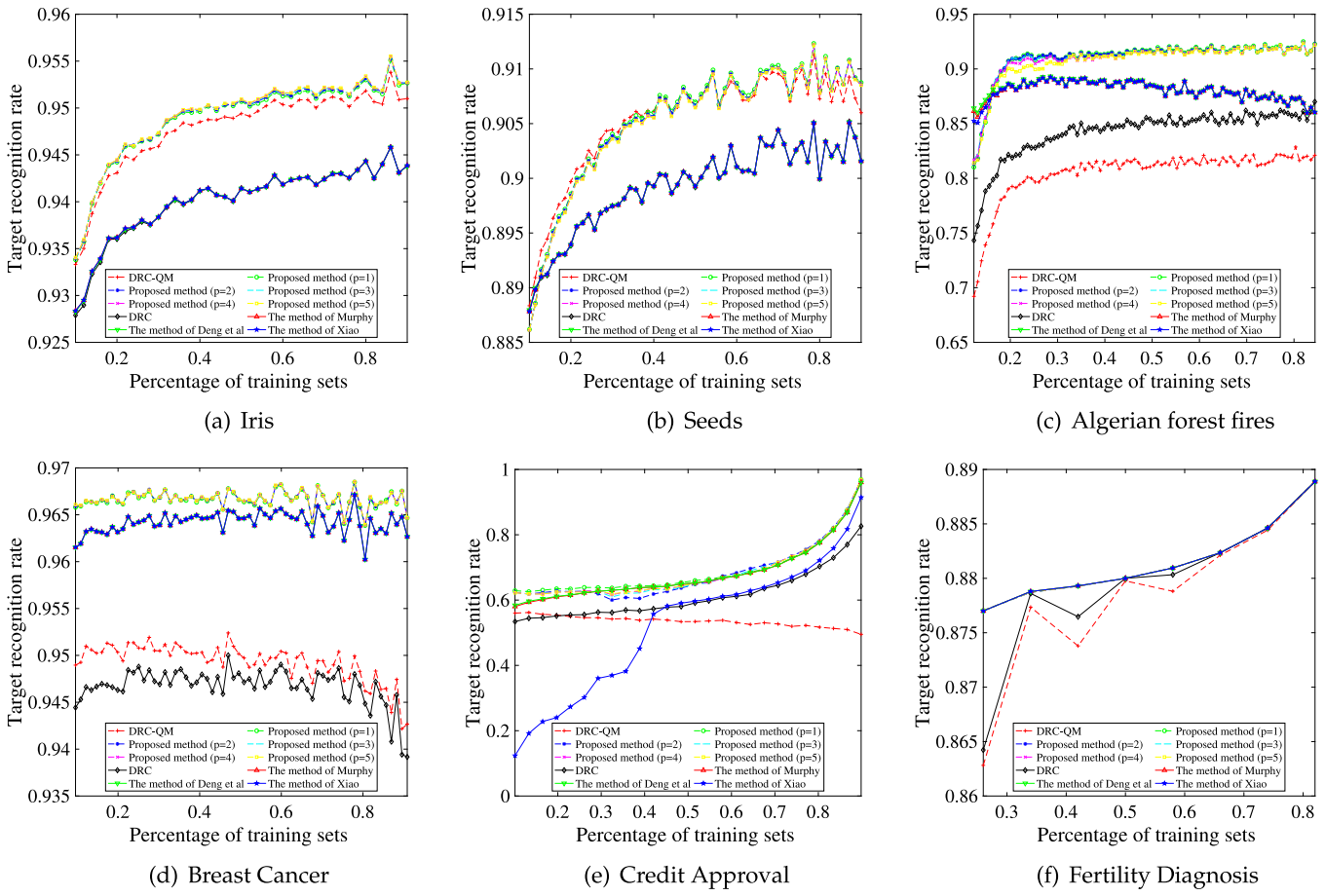

Fig. 9. The accuracy of target recognition changes with the increase of the number of training sets.

Algorithm 1 Multi-source information fusion based on discount coefficient

Input: N bodies of evidence.
Output: Recognized target

```
for k = 1 → n do
    for l = 1 → n do
        Conduct distance matrix based on Eq (8) and (9)
    end for
end for
for k = 1 → n do
    Calculate the support degree though Eq (10)
end for
for k = 1 → n do
    Generate the discount coefficient based on Eq (11)
end for
for k = 1 → n do
    Generate the discount mass functions though Eq (12)
end for
for k = 1 → n do
    Normalize the discount mass function
end for
Fuses multiple-sources information though Step 6
return result of Step 7
```

Scheme description: We sequentially increase the number of training sets sequentially, then generate the mass functions using the method in Pan and Den (2022), and conduct the Monte Carlo validation experiment 100 times. The experimental results of different methods based on the data sets are shown in Fig. 9. Moreover, to explain the proposed fusion method, we chose the last data point of the 100th time when the number of training sets is 45 as test point to illustrate the fusion process in the context of the iris data sets. According to the method in Pan and Den (2022), this test point generates the following mass functions:

Sepal length (SL):

$\mathbb{M}_{SL}(Set) = 0.3651 - 0.0102i$, $\mathbb{M}_{SL}(Ver) = 0.3803 - 0.0032i$, $\mathbb{M}_{SL}(Virg) = 0.3795 + 0.0027i$ $\mathbb{M}_{SL}(Set, Ver) = 0.3803 - 0.0035i$ $\mathbb{M}_{SL}(Set, Virg) = 0.3798 - 0.0020i$, $\mathbb{M}_{SL}(Ver, Virg) = 0.3799 - 0.0001i$ $\mathbb{M}_{SL}(Set, Ver, Virg) = 0.3804 - 0.0013i$

Sepal width (SW):

$\mathbb{M}_{SW}(Set) = 0.3752 + 0.0059i$, $\mathbb{M}_{SW}(Ver) = 0.3776 + 0.0004i$ $\mathbb{M}_{SW}(Virg) = 0.3787 + 0.0023i$, $\mathbb{M}_{SW}(Set, Ver) = 0.3785 + 0.0016i$ $\mathbb{M}_{SW}(Set, Virg) = 0.3785 + 0.0021i$, $\mathbb{M}_{SW}(Ver, Virg) = 0.3784 + 0.0007i$ $\mathbb{M}_{SW}(Set, Ver, Virg) = 0.3787 + 0.0010i$

Petal length (PL):

$\mathbb{M}_{PL}(Set) = 0.2750 - 0.0206i$, $\mathbb{M}_{PL}(Ver) = 0.3925 - 0.0057i$ $\mathbb{M}_{PL}(Virg) = 0.3932 + 0.0056i$, $\mathbb{M}_{PL}(Set, Ver) = 0.3912 - 0.0088i$ $\mathbb{M}_{PL}(Set, Virg) = 0.3918 - 0.0060i$, $\mathbb{M}_{PL}(Ver, Virg) = 0.3926 - 0.0000i$ $\mathbb{M}_{PL}(Set, Ver, Virg) = 0.3930 - 0.0033i$

Petal width (PW):

$\mathbb{M}_{PW}(Set) = 0.3329 - 0.0113i$, $\mathbb{M}_{PW}(Ver) = 0.3825 - 0.0040i$ $\mathbb{M}_{PW}(Virg) = 0.3862 + 0.0020i$, $\mathbb{M}_{PW}(Set, Ver) = 0.3838 - 0.0043i$ $\mathbb{M}_{PW}(Set, Virg) = 0.3854 - 0.0028i$, $\mathbb{M}_{PW}(Ver, Virg) = 0.3856 - 0.0005i$ $\mathbb{M}_{PW}(Set, Ver, Virg) = 0.3860 - 0.0017i$.

Step 1 : Generate the distance measure matrix (p=2):

$$\overline{M} = \begin{bmatrix} 0 & 0.0274 & 0.0715 & 0.0259 \\ 0.0274 & 0 & 0.0892 & 0.0448 \\ 0.0715 & 0.0892 & 0 & 0.0466 \\ 0.0259 & 0.0448 & 0.0466 & 0 \end{bmatrix}$$

Step 2 : Calculate the support degree of each body of evidence:

$\overline{Sup_{\mathbb{M}_{SL}}} = 2.8753$, $\overline{Sup_{\mathbb{M}_{SW}}} = 2.8387$, $\overline{Sup_{\mathbb{M}_{PL}}} = 2.7928$, $\overline{Sup_{\mathbb{M}_{PW}}} = 2.8828$

Step 3 : Generate the discount coefficient:

$\overline{\alpha_{SL}} = 0.5024$, $\overline{\alpha_{SW}} = 0.4992$, $\overline{\alpha_{PL}} = 0.4952$, $\overline{\alpha_{PW}} = 0.5031$

Step 4 : Calculate the discount mass function:

$\overline{\alpha_{SL}}\mathbb{M}_{SL}(Set) = 0.1835 - 0.0051i$, $\overline{\alpha_{SL}}\mathbb{M}_{SL}(Ver) = 0.1911 - 0.0016i$, $\overline{\alpha_{SL}}\mathbb{M}_{SL}(Virg) = 0.1907 + 0.0013i$, $\overline{\alpha_{SL}}\mathbb{M}_{SL}(Set, Ver) = 0.1911 - 0.0018i$ $\overline{\alpha_{SL}}\mathbb{M}_{SL}(Set, Virg) = 0.1908 - 0.0010i$, $\overline{\alpha_{SL}}\mathbb{M}_{SL}(Ver, Virg) = 0.1909 - 0.0001i$, $\overline{\alpha_{SL}}\mathbb{M}_{SL}(Set, Ver, Virg) = 2.3387 - 0.0154i$

$\overline{\alpha_{SW}}\mathbb{M}_{SW}(Set) = 0.1873 + 0.0030i$, $\overline{\alpha_{SW}}\mathbb{M}_{SW}(Ver) = 0.1885 + 0.0002i$, $\overline{\alpha_{SW}}\mathbb{M}_{SW}(Virg) = 0.1891 + 0.0011i$, $\overline{\alpha_{SW}}\mathbb{M}_{SW}(Set, Ver) = 0.1890 + 0.0008i$, $\overline{\alpha_{SW}}\mathbb{M}_{SW}(Set, Virg) = 0.189 + 0.001i$, $\overline{\alpha_{SW}}\mathbb{M}_{SW}(Ver, Virg) = 0.1889 + 0.0003i$, $\overline{\alpha_{SW}}\mathbb{M}_{SW}(Set, Ver, Virg) = 2.3430 + 0.0121i$

$\overline{\alpha_{PL}}\mathbb{M}_{PL}(Set) = 0.1362 - 0.0102i$, $\overline{\alpha_{PL}}\mathbb{M}_{PL}(Ver) = 0.1944 - 0.0028i$, $\overline{\alpha_{PL}}\mathbb{M}_{PL}(Virg) = 0.1947 + 0.0028i$, $\overline{\alpha_{PL}}\mathbb{M}_{PL}(Set, Ver) = 0.1937 - 0.0044i$, $\overline{\alpha_{PL}}\mathbb{M}_{PL}(Set, Virg) = 0.1940 - 0.0030i$, $\overline{\alpha_{PL}}\mathbb{M}_{PL}(Ver, Virg) = 0.1944 - 0.0000i$,

$\overline{\alpha_{PW}}\mathbb{M}_{PW}(Set) = 0.1675 - 0.0057i$, $\overline{\alpha_{PW}}\mathbb{M}_{PW}(Ver) = 0.1924 - 0.0020i$, $\overline{\alpha_{PW}}\mathbb{M}_{PW}(Virg) = 0.1943 + 0.0010i$, $\overline{\alpha_{PW}}\mathbb{M}_{PW}(Set, Ver) = 0.1931 - 0.0022i$, $\overline{\alpha_{PW}}\mathbb{M}_{PW}(Set, Virg) = 0.1939 - 0.0014i$, $\overline{\alpha_{PW}}\mathbb{M}_{PW}(Ver, Virg) = 0.194 - 0.0003i$, $\overline{\alpha_{PW}}\mathbb{M}_{PW}(Set, Ver, Virg) = 2.3361 - 0.0197i$.

Step 5 : Normalize the discount mass function :

$\overline{\alpha_{SL}}\mathbb{M}_{SL}(Set) = 0.0769 - 0.0022i$, $\overline{\alpha_{SL}}\mathbb{M}_{SL}(Ver) = 0.0801 - 0.0007i$, $\overline{\alpha_{SL}}\mathbb{M}_{SL}(Virginica) = 0.0800 + 0.0006i$, $\overline{\alpha_{SL}}\mathbb{M}_{SL}(Set, Ver) = 0.0801 - 0.0007i$, $\overline{\alpha_{SL}}\mathbb{M}_{SL}(Set, Virg) = 0.0800 - 0.0004i$, $\overline{\alpha_{SL}}\mathbb{M}_{SL}(Ver, Virg) = 0.0800 - 0.0000ii$, $\overline{\alpha_{SL}}\mathbb{M}_{SL}(Set, Ver, Virg) = 0.9808 - 0.0065i$

$\overline{\alpha_{SW}}\mathbb{M}_{SW}(Set) = 0.0784 + 0.0012i$, $\overline{\alpha_{SW}}\mathbb{M}_{SW}(Ver) = 0.0789 + 0.0001i$, $\overline{\alpha_{SW}}\mathbb{M}_{SW}(Virg) = 0.0792 + 0.0005i$, $\overline{\alpha_{SW}}\mathbb{M}_{SW}(Set, Ver) = 0.0791 + 0.0003i$, $\overline{\alpha_{SW}}\mathbb{M}_{SW}(Set, Vir) = 0.0791 + 0.0004i$, $\overline{\alpha_{SW}}\mathbb{M}_{SW}(Ver, Vir) = 0.0791 + 0.0001i$, $\overline{\alpha_{SW}}\mathbb{M}_{SW}(Set, Ver, Virg) = 0.9811 + 0.0051i$

$\overline{\alpha_{PL}}\mathbb{M}_{PL}(Set) = 0.0572 - 0.0043i$, $\overline{\alpha_{PL}}\mathbb{M}_{PL}(Ver) = 0.0817 - 0.0012i$, $\overline{\alpha_{PL}}\mathbb{M}_{PL}(Virginica) = 0.0818 + 0.0012i$, $\overline{\alpha_{PL}}\mathbb{M}_{PL}(Set, Ver) = 0.0814 - 0.0018i$, $\overline{\alpha_{PL}}\mathbb{M}_{PL}(Set, Virg) = 0.0815 - 0.0012i$, $\overline{\alpha_{PL}}\mathbb{M}_{PL}(Ver, Virg) = 0.0817 - 0.0000i$, $\overline{\alpha_{PL}}\mathbb{M}_{PL}(Set, Ver, Virg) = 0.9814 - 0.0144i$

$\overline{\alpha_{PW}}\mathbb{M}_{PW}(Set) = 0.0703 - 0.0024i$, $\overline{\alpha_{PW}}\mathbb{M}_{PW}(Ver) = 0.0808 - 0.0008i$, $\overline{\alpha_{PW}}\mathbb{M}_{PW}(Virg) = 0.0816 + 0.0004i$, $\overline{\alpha_{PW}}\mathbb{M}_{PW}(Set, Ver) = 0.0811 - 0.0009i$, $\overline{\alpha_{PW}}\mathbb{M}_{PW}(Set, Vir) = 0.0814 - 0.0006i$, $\overline{\alpha_{PW}}\mathbb{M}_{PW}(Ver, Vir) = 0.0814 - 0.0001i$, $\overline{\alpha_{PW}}\mathbb{M}_{PW}(Set, Ver, Virg) = 0.9808 - 0.0083i$.

Step 6 : Combine N discount mass functions in turn:

$\overline{CM}(Set) = 0.3636 + 0.0117i$, $\overline{CM}(Ver) = 0.4099 + 0.0066i$, $\overline{CM}(Virg) = 0.4112 + 0.0041i$, $\overline{CM}(Set, Ver) = 0.2270 + 0.0045i$, $\overline{CM}(Set, Virg) = 0.2273 + 0.0041i$, $\overline{CM}(Ver, Virg) = 0.2275 + 0.0030i$, $\overline{CM}(Set, Ver, Virg) = 0.6127 + 0.0110i$.

Step 7 : Though PPT rule to transformed $\overline{CM}$:

$\overline{PPT}(Set) = 0.6324$, $\overline{PPT}(Ver) = 0.7080$, $\overline{PPT}(Virg) = 0.7105$

It is evident that the unknown target is Virginica. According to the query results, the location of the test point in the data set corresponds to the Virginica. In this regard, it shows that the proposed fusion method is capable of recognizing unknown targets effectively.

As shown in Fig. 9, we add the experimental results of the existing method, which provide a better verification of the performance of the proposed fusion method. Fig. 9(a) shows the accuracy of unknown target recognition in iris data set. As can be seen from the figure, the accuracy of all methods increases with the increase of the number of training sets. It should be noted that regardless of how p changes, the proposed fusion method is more accurate than other methods, such as DRC-QM, Dempster rule of combination (DRC), Murphy's method. Fig. 9(b) reflects the change of the accuracy rate of unknown target recognition as the number of training sets increases in the Seeds data set. It can be seen from the figure that the accuracy of the all methods increases with the increase of the number of training sets. Compared with other methods, the proposed fusion method has a higher recognition rate. Also, the proposed method offers greater advantages in identifying unknown targets in Algerian Forest Fires and Breast Cancer (See Fig. 9(c) and (d)). In the Credit Approval data set, there are missing data points, so the training set deletes those data points, while in the test set, the missing data points correspond to propositions with maximum uncertainty. This leads to the recognition rate of DRC-QM to unknown targets decreases with the increase of training sets. However, as for the proposed fusion method, its recognition rate remains the highest (See Fig. 9(e)). With Fertility Diagnosis data set, the recognition rates of all methods are roughly the same (See Fig. 9(f)). In conclusion, it can be found in six data set experiments that compare with existing methods the proposed method has good recognition performance in data set environment.

It is important to note, that this paper also analyzes the computational complexity of the proposed fusion method, as shown in Fig. 10. There is a close correspondence between the computational complexity of these methods and the computational complexity of their combination rules (DRC or DRC-QM). Actually, the computational complexity of these methods depends on the complexity of the combination rules, but there are some subtle differences between different methods. To explain it, two experiments are designed. In the corresponding experimental scheme in Fig. 10(a), the size of the frame of discernment is set as 3, and each method is performed 100 times. Fig. 10(a) reflects the trend that the running time of each method changes as the number of mass functions increases. Intuitively, the running time of each method and the number of mass functions generally follow a linear relationship, but there are some differences. It should be noted that, when the size of the frame of discernment is determined in the real plane, the running time of DRC is only determined by the computational complexity of DRC, resulting in a minimal running time. Xiao's method and Murphy's method have longer running times than DRC, as some basic operations are required in addition to the running time of DRC. Deng et al.'s method has the highest running time in the real plane. Since it involves evidence distance, it will increase the running time more than the previous three methods. Additionally, the running time of QRC-QM in the complex plane is much shorter than that of the proposed fusion method. It is imperative to note that the proposed fusion method introduce QMD, as well as some other basic operations, including but not limited to complex operations. This results in the proposed fusion method having the longest running time when compared to other methods. In the experimental scheme corresponding to Fig. 10(b), the number of mass functions is set to 2, and each method is performed 50 times. Fig. 10(b) depicts the trend of the average running time of each method as the size of the frame of discernment increases. Obviously, the running time increases exponentially as the size of the frame of discernment increases, which is reasonable. Because DRC/DRC-QM is the core step of each method in the real/complex plane, their running time makes up a substantial portion of each method's running time. Therefore, the running time of each method increases exponentially as the size of the frame of discernment increases, but there are some differences. Among these methods, the DRC has the shortest running time, followed by the DRC-QM, and the proposed fusion method has the longest running time. Since the proposed fusion method involves a number of other basic operations in addition to DRC-QM, which require time to complete. The proposed method can, therefore, be improved from the following two perspectives once it is applied in the field with real-time monitoring. To begin with, reduce as much as possible the redundant propositions within the mass function. Secondly, DRC-QM is replaced by a simpler matrix operation.

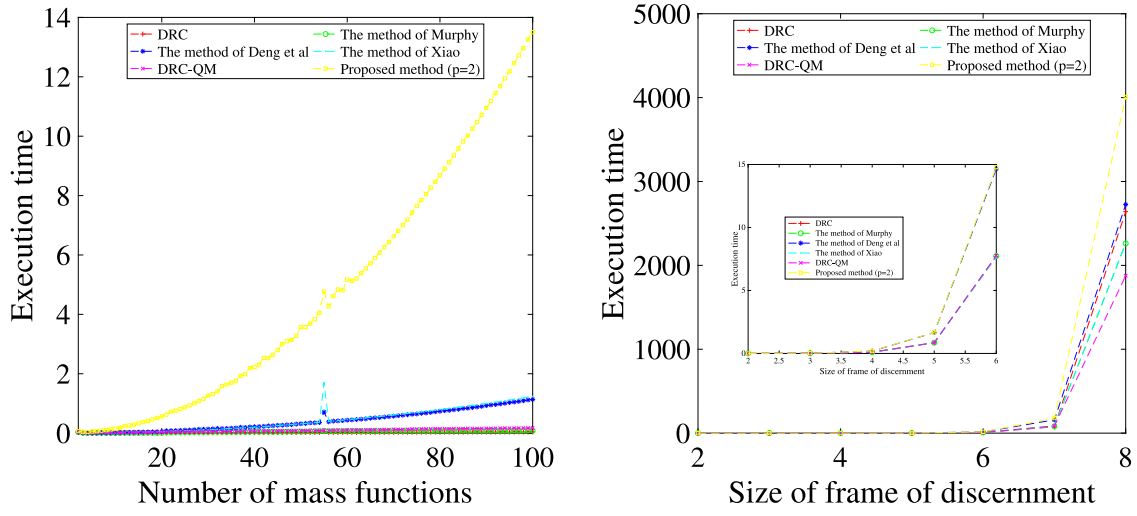

(a) The tendency of the running time to change with the increasing number of mass functions

(b) The tendency of the running time to change with the increase of the sixe of frame of discernment

Fig. 10. Influence of different factors on running time.

4. Conclusion and future work

In this paper, based on the idea of evidence distance and Minkowski distance, a distance of quantum mass function is defined, abbreviated as QMD. As well as being a strict distance measure, QMD solves the issue of measuring the difference between mass functions in the complex plane that is not possible with traditional distance measures. Additionally, with the aid of QMD, a multi-source information fusion method based on the discount coefficient is developed. Finally, the multi-source information fusion method is applied to the recognition of unknown targets in the data sets environment. Experimental results indicate that the proposed fusion method has a higher recognition rate than the existing methods.

As QMD introduces Minkowski distance in the complex plane, it has the advantage of Minkowski distance. Therefore, the value of the parameter p must be considered. In practical applications, p can be generated through training sets It is generally accepted that each type of data set has a corresponding parameter p. It is recommended to set parameter p as small as possible in the condition that the performance of the proposed fusion method remains unchanged. Moreover, the second limitation of the proposed fusion approach is the increased complexity of the computations involved. QMD introduces the idea of evidence distance, which leads to the maximum time cost of the proposed fusion method compared with other classical fusion methods. As a result, one of the future research directions for this paper is to reduce the computational complexity of the proposed fusion method by simplifying the structure of the proposition in the quantum mass function. The second future work is to apply the proposed fusion method to real world scenarios with periodic characteristics to assist with decision making, including but not limited to garbage collection and disposal (Wang and Wang, 2022).

CRediT authorship contribution statement

Lipeng Pan: Conceptualization, Methodology, Writing – original draft, Writing – review & editing. **Xiaozhuan Gao:** Writing – original draft, Writing – review & editing. **Yong Deng:** Validation, Resources, Writing – review & editing, Supervision, Funding acquisition.

Declaration of competing interest

The authors declare that they have no known competing financial interests or personal relationships that could have appeared to influence the work reported in this paper.

Data availability

No data was used for the research described in the article.

Acknowledgments

The work is partially supported by National Natural Science Foundation of China (Grant No. 61973332), JSPS Invitational Fellowships for Research in Japan (Short-term).

References

Alkouri, A.M.J.S., Salleh, A.R., 2012. Complex intuitionistic fuzzy sets. In: AIP Conference Proceedings. Vol. 1482, (1), American Institute of Physics, pp. 464–470.

Bouhamed, S.A., Kallel, I.K., Yager, R.R., Bossé, É., Solaiman, B., 2020. An intelligent quality-based approach to fusing multi-source possibilistic information. Inf. Fusion 55, 68–90.

Buono, F., Longobardi, M., 2020. A dual measure of uncertainty: The deng extropy. Entropy 22 (5), http://dx.doi.org/10.3390/e22050, URL https://www.mdpi.com/1099-4300/22/5/582.

Cao, Z., John, A.R., Chen, H.-T., Martens, K.E., Georgiades, M., Gilat, M., Nguyen, H.T., Lewis, S.J., Lin, C.-T., 2021a. Identification of EEG dynamics during freezing of gait and voluntary stopping in patients with Parkinson's disease. IEEE Trans. Neural Syst. Rehabil. Eng. 29, 1774–1783.

Cao, Z., Wong, K., Lin, C.-T., 2021b. Weak human preference supervision for deep reinforcement learning. IEEE Trans. Neural Netw. Learn. Syst. 32 (12), 5369–5378.

Chang, L., Dong, W., Yang, J., Sun, X., Xu, X., Xu, X., Zhang, L., 2020. Hybrid belief rule base for regional railway safety assessment with data and knowledge under uncertainty. Inform. Sci. 518, 376–395.

Che, Y., Deng, Y., Yuan, Y.-H., 2022. Maximum-entropy-based decision-making trial and evaluation laboratory and its application in emergency management. J. Organ. End User Comput. (JOEUC) 34 (7), 1–16.

Chen, Z., Cai, R., 2022. Updating incomplete framework of target recognition database based on fuzzy gap statistic. Eng. Appl. Artif. Intell. 107, 104521.

Chen, X., Deng, Y., 2022. An evidential software risk evaluation model. Mathematics 10 (13), http://dx.doi.org/10.3390/math10132325.

Cui, H., Zhou, L., Li, Y., Kang, B., 2022. Belief entropy-of-entropy and its application in the cardiac interbeat interval time series analysis. Chaos Solitons Fractals 155, 111736. http://dx.doi.org/10.1016/j.chaos.2021.111736.

Cuzzolin, F., 2020. The Geometry of Uncertainty: The Geometry of Imprecise Probabilities. Springer Nature.

Dempster, A.P., 1967. Upper and lower probabilities induced by a multivalued mapping. Ann. Math. Stat. 38 (2), 325–339.
Deng, Y., 2022. Random permutation set. Int. J. Comput., Commun. Control 17 (1).
Deng, Z., Wang, J., 2021. A new evidential similarity measurement based on Tanimoto measure and its application in multi-sensor data fusion. Eng. Appl. Artif. Intell. 104, 104380.
Dong, Y., Li, X., Dezert, J., Khyam, M.O., Noor-A-Rahim, M., Ge, S.S., 2020. Dezert-Smarandache theory-based fusion for human activity recognition in body sensor networks. IEEE Trans. Ind. Inf. 16 (11), 7138–7149.
Dong, Y., Li, X., Dezert, J., Zhou, R., Zhu, C., Wei, L., Ge, S.S., 2021. Evidential reasoning with hesitant fuzzy belief structures for human activity recognition. IEEE Trans. Fuzzy Syst. 29 (12), 3607–3619.
Fu, C., Xue, M., Liu, W., Xu, D., Yang, J., 2021. Data-driven preference learning in multiple criteria decision making in the evidential reasoning context. Appl. Soft Comput. 102, 107109.
Gao, X., Deng, Y., 2019. Quantum model of mass function. Int. J. Intell. Syst. 35, 267–282.
Gao, X., Deng, Y., 2021. Generating method of Pythagorean fuzzy sets from the negation of probability. Eng. Appl. Artif. Intell. 105, 104403.
Gao, X., Pan, L., Deng, Y., 2021a. Quantum pythagorean fuzzy evidence theory (QPFET): A negation of quantum mass function view. IEEE Trans. Fuzzy Syst. http://dx.doi.org/10.1109/TFUZZ.2021.3057993.
Gao, X., Pan, L., Deng, Y., 2022. A generalized divergence of information volume and its applications. Eng. Appl. Artif. Intell. 108, 104584.
Gao, F., Tan, S., Shi, H., Mu, Z., 2021b. A status-relevant blocks fusion approach for operational status monitoring. Eng. Appl. Artif. Intell. 106, 104455.
Gao, Q., Wen, T., Deng, Y., 2021c. Information volume fractal dimension. Fractals 29 (08), 2150263. http://dx.doi.org/10.1142/S0218348X21502637.
Ghosh, N., Saha, S., Paul, R., 2021. iDCR: Improved Dempster combination rule for multisensor fault diagnosis. Eng. Appl. Artif. Intell. 104, 104369.
Janani, K., Veerakumari, K.P., Vasanth, K., Rakkiyappan, R., 2022. Complex Pythagorean fuzzy einstein aggregation operators in selecting the best breed of Horsegram. Expert Syst. Appl. 187, 115990.
Jousselme, A.-L., Grenier, D., Bossé, É., 2001. A new distance between two bodies of evidence. Inf. Fusion 2 (2), 91–101.
Jousselme, A.-L., Maupin, P., 2012. Distances in evidence theory: Comprehensive survey and generalizations. Internat. J. Approx. Reason. 53 (2), 118–145.
Jousselme, A.-L., Pichon, F., Ben Abdallah, N., Destercke, S., 2021. A note about entropy and inconsistency in evidence theory. In: International Conference on Belief Functions. Springer, pp. 215–223.
Ju, H., Ding, W., Yang, X., Fujita, H., Xu, S., 2021. Robust supervised rough granular description model with the principle of justifiable granularity. Appl. Soft Comput. 110, 107612.
Khalaj, M., Tavakkoli-Moghaddam, R., Khalaj, F., Siadat, A., 2020. New definition of the cross entropy based on the Dempster-Shafer theory and its application in a decision-making process. Comm. Statist. Theory Methods 49 (4), 909–923.
Laplace, P.-S., 1812. Analytical theory of probabilities. Published in.
Liao, H., Ren, Z., Fang, R., 2020. A deng-entropy-based evidential reasoning approach for multi-expert multi-criterion decision-making with uncertainty. Int. J. Comput. Intell. Syst. 13 (1), 1281–1294.
Liu, Z.-G., Liu, Y., Dezert, J., Cuzzolin, F., 2020. Evidence combination based on credal belief redistribution for pattern classification. IEEE Trans. Fuzzy Syst. 28 (4), 618–631. http://dx.doi.org/10.1109/TFUZZ.2019.2911915.
Mahmood, T., Ur Rehman, U., 2022. A novel approach towards bipolar complex fuzzy sets and their applications in generalized similarity measures. Int. J. Intell. Syst. 37 (1), 535–567.
Mi, X., Kang, B., 2020. On the belief universal gravitation (BUG). Comput. Ind. Eng. 148, 106685.
Pan, L., Den, Y., 2022. A new complex evidence theory. Inform. Sci. http://dx.doi.org/10.1016/j.ins.2022.06.063.
Porebski, S., Porwik, P., Straszecka, E., Orczyk, T., 2018. Liver fibrosis diagnosis support using the Dempster–Shafer theory extended for fuzzy focal elements. Eng. Appl. Artif. Intell. 76, 67–79.
Ramot, D., Milo, R., Friedman, M., Kandel, A., 2002. Complex fuzzy sets. IEEE Trans. Fuzzy Syst. 10 (2), 171–186.
Sarabi-Jamab, A., Araabi, B.N., 2018. How to decide when the sources of evidence are unreliable: A multi-criteria discounting approach in the Dempster–Shafer theory. Inform. Sci. 448, 233–248.
Shafer, G., 1976. A Mathematical Theory of Evidence. Vol. 42, Princeton University Press.
Solaiman, B., Guériot, D., Almouahed, S., Alsahwa, B., Bossé, É., 2021. A new hybrid possibilistic-probabilistic decision-making scheme for classification. Entropy 23 (1), 67.
Song, M., Sun, C., Cai, D., Hong, S., Li, H., 2022. Classifying vaguely labeled data based on evidential fusion. Inform. Sci. 583, 159–173.
Song, X., Xiao, F., 2022. Combining time-series evidence: A complex network model based on a visibility graph and belief entropy. Appl. Intell. http://dx.doi.org/10.1007/s10489--021--02956--5.
Surathong, S., Auephanwiriyakul, S., Theera-Umpon, N., 2018. Decision fusion using fuzzy Dempster-Shafer theory. In: International Conference on Computing and Information Technology. Springer, pp. 115–125.
Ullah, K., Mahmood, T., Ali, Z., Jan, N., 2020. On some distance measures of complex Pythagorean fuzzy sets and their applications in pattern recognition. Complex Intell. Syst. 6 (1), 15–27.
Wang, H., Deng, X., Jiang, W., Geng, J., 2021a. A new belief divergence measure for Dempster–Shafer theory based on belief and plausibility function and its application in multi-source data fusion. Eng. Appl. Artif. Intell. 97, 104030.
Wang, H., Fang, Y.-P., Zio, E., 2022a. Resilience-oriented optimal post-disruption reconfiguration for coupled traffic-power systems. Reliab. Eng. Syst. Saf. 222, 108408. http://dx.doi.org/10.1016/j.ress.2022.108408.
Wang, H., Liao, H., Xu, Z., 2021b. Order relations and operations on the set of probabilistic linguistic term sets. IEEE Trans. Fuzzy Syst. 30 (5), 1475–1485.
Wang, T., Liu, W., Cabrera, L.V., Wang, P., Wei, X., Zang, T., 2022b. A novel fault diagnosis method of smart grids based on memory spiking neural p systems considering measurement tampering attacks. Inform. Sci. 596, 520–536. http://dx.doi.org/10.1016/j.ins.2022.03.013, URL https://www.sciencedirect.com/science/article/pii/S0020025522002122.
Wang, L., Wang, H., 2022. An integrated qualitative group decision-making method for assessing health-care waste treatment technologies based on linguistic terms with weakened hedges. Appl. Soft Comput. 117, 108435.
Wang, H., Yu, D., Xu, Z., 2021c. A novel process to determine consensus thresholds and its application in probabilistic linguistic group decision-making. Expert Syst. Appl. 168, 114315.
Xiao, F., 2019. Multi-sensor data fusion based on the belief divergence measure of evidences and the belief entropy. Inf. Fusion 46, 23–32.
Xiao, F., 2020. CED: A distance for complex mass functions. IEEE Trans. Neural Netw. Learn. Syst. 32 (4), 1525–1535.
Xiao, F., Pedrycz, W., 2022. Negation of the quantum mass function for multisource quantum information fusion with its application to pattern classification. IEEE Trans. Pattern Anal. Mach. Intell. http://dx.doi.org/10.1109/TPAMI.2022.3167045.
Xiao, F., Wen, J., Pedrycz, W., 2022. Generalized divergence-based decision making method with an application to pattern classification. IEEE Trans. Knowl. Data Eng. http://dx.doi.org/10.1109/TKDE.2022.3177896.
Xiaojing, F., Deqiang, H., Yi, Y., Dezert, J., 2022. De-combination of belief function based on optimization. Chin. J. Aeronaut. 35 (5), 179–193.
Xiong, L., Su, X., Qian, H., 2021. Conflicting evidence combination from the perspective of networks. Inform. Sci. 580, 408–418. http://dx.doi.org/10.1016/j.ins.2021.08.088.
Yager, R.R., 2022. Aggregating ordinal values using a measure based median. Inf. Fusion 78, 86–89.
Yan, Z., Zhao, H., Mei, X., 2021. An improved conflicting-evidence combination method based on the redistribution of the basic probability assignment. Appl. Intell. 1–27.
Yi, Y., Deqiang, H., Dezert, J., 2019. Basic belief assignment approximations using degree of non-redundancy for focal element. Chin. J. Aeronaut. 32 (11), 2503–2515.
Zadeh, L.A., 1965. Fuzzy sets. Inf. Control 8 (3), 338–353.
Zhu, C., Xiao, F., 2021. A belief Hellinger distance for D–S evidence theory and its application in pattern recognition. Eng. Appl. Artif. Intell. 106, 104452.